Commun. Theor. Phys. (Beijing, China) **50** (2008) pp. 719–724

Vol. 50, No. 3, September 15, 2008

CDCC Approaches and Roles of Closed Channels in *d*-Nucleus Reactions

AN Hai-Xia* and CAI Chong-Hai

Department of Physics, Nankai University, Tianjin 300071, China

(Received October 17, 2007; Revised December 11, 2007)

Abstract *The effect of deuteron breakup in d-nucleus reaction is treated with the continuum discretized coupled channels (CDCC) approach, and the effects on the total reaction cross sections and elastic scattering angular distributions are studied by comparing the calculations of CDCC and spherical optical model with our global deuteron optical potential [Phys. Rev. C* **73** *(2006) 054605] below 200 MeV, for target nuclei ranging from* ^{12}C *to* ^{208}Pb*. The contributions from the closed channels to the total reaction and breakup cross sections, and angular distributions of elastic scattering are also seriously discussed.*

PACS numbers: 24.10.Eq
Key words: CDCC approach, closed channel, spherical optical model, global deuteron optical potential

1 Introduction

The elastic scattering of deuteron is of particular interest in nuclear reaction studies as the scattering of the simplest kind of composite particle. Several studies have used a spherical optical model framework for searching for the phenomenological global deuteron optical potential[1−5] to reproduce the elastic scattering angular distributions and reaction cross sections, and all of these studies are based on the large numbers of experimental data of the target nuclei in some (Z, A) range. Both the latest two sets of global deuteron optical potential parameters[1,2] can fit the experimental data very well for almost all target nuclei ranging from ^{12}C to ^{238}U in the energy region below 200 MeV. However, the deuteron is a weakly bound nucleus with a binding energy of only 2.2259 MeV and it is well known that it easily breaks up in nuclear collisions. The deuteron breakup is an important process with significant effects on the elastic and inelastic channels. The CDCC approach has been successful in describing the nuclear reactions with weakly bound particle as projectile or an outgoing particle. Up to now, there are a lot of research on deuteron breakup and the CDCC approach, such as Refs. [6] ∼ [19].

In CDCC approach, when the *p*-*n* pair relative kinetic energy is larger than the total energy of the *n*-*p*-*A* three-body system, according to the total energy conservation of this system, the relative kinetic energy of the center of mass of the deuteron moving against the target nucleus is negative, and the channel with negative relative kinetic energy is called as closed channel. When the *p*-*n* pair relative kinetic energy is smaller than the total energy of the *n*-*p*-*A* system, then the relative kinetic energy of the c.m. of the deuteron moving against the target nucleus is positive, and the channel with positive energy is called as open channel. One should keep in mind that the *p*-*n* pair relative kinetic energy is always positive in CDCC. Although these negative energy states cannot be observed in experiments, the closed channels are coupled to the open channels and affect their properties. N. Austern pointed out[7] that the closed channels would make large contributions to the stripping reactions in low energy region. However, most CDCC calculations did not include the contributions of the closed channels to the reaction cross sections σ_R, breakup cross sections σ_b and elastic scattering angular distributions. They only took open channels into account. Thus, it is necessary to study the contributions of the closed channels and those of the deuteron breakup effects on σ_R, σ_b and elastic scattering angular distributions. And the roles of the closed channels are emphasized in this work.

For the Coulomb potential, some calculations neglect it[15−18] and some consider it depending on the coordinate of the c.m. of deuteron R instead of the coordinate of proton r_p.[9,19] Actually, in the three-body model it should depend on r_p rather than R, and this treatment would more truly reflect the real physical picture. In this work, both the open channels and closed channels are calculated with the Coulomb potential at r_p, but the Coulomb potential is ignored in the non-diagonal elements for closed channels. As for the nuclear potentials of the nucleon-target interaction of the three-body model, Koning–Delaroche's global p, n potential parameters[20] are used in this work.

The purpose of this paper is to observe the effects of deuteron breakup on the reaction cross sections and elastic scattering angular distributions by comparing the results of CDCC optical model and those of spherical optical model with our global potential parameters. Systematical discussing and analyzing the contributions of closed channels is the essential of this work.

This paper is arranged as follows. In Sec. 2 we begin with the theoretical formalism, the CDCC approach is briefly reviewed, and truncation of model space is described. In Sec. 3, the validity of the calculation method used in this work is tested firstly; and then the roles of the closed channels are systematically discussed; at last, numerical results and discussions are presented. Section 4 is a summary.

2 Theoretical Formalism

Neglecting the total anti-symmetrization, target excitation, and the spin of p, n and the target nucleus, the Hamiltonian of the $(A+2)$ system can be described as[7,8]

$$H = K_{\vec{R}} + U_{nA}(\vec{r}_{nA}) + U_{pA}(\vec{r}_{pA}) + U^{\rm Coul}(\vec{r}_{pA}) + H_{pn}\,, \quad (1)$$

$$H_{pn} = K_{\vec{r}} + V_{pn}(\vec{r})\,, \quad (2)$$

*E-mail: anhaixia@mail.nankai.edu.cn

where $V_{pn}(\vec{r})$ is the interaction between p and n, which is chosen as a Gaussian form:

$$V_{pn}(r) = -v_0 \exp\Big[-\Big(\frac{r}{r_0}\Big)^2\Big] \tag{3}$$

with $v_0 = 72.194$ MeV and $r_0 = 1.484$ fm. The vector $\vec{r}$ is a coordinate of p relative to n, and $\vec{R}$ is the coordinate of the center of mass of the p-n pair relative to target nucleus A, namely, $\vec{r} = \vec{r}_{pA} - \vec{r}_{nA}$, $\vec{R} = (\vec{r}_{pA} + \vec{r}_{nA})/2$. Figure 1 describes all the position vectors of this $(A+2)$ system. The U_{nA}, U_{pA} are the nucleon-target optical potentials, and they are assumed to be the central part of the n, p optical potential at half the deuteron incident energy, and the spin-orbital coupling potentials are ignored. The $U^{\rm Coul}(\vec{r}_{pA})$ is the Coulomb potential of proton in deuteron relative to target nucleus. The operators $K_{\vec{r}}$, $K_{\vec{R}}$ are the kinetic energies associated with $\vec{r}$ and $\vec{R}$, respectively.

The complete set of orthonormalized eigenfunctions of p-n Hamiltonian satisfies:

$$(H_{pn} - \varepsilon_0)\phi_0(\vec{r}) = 0\,, \quad \varepsilon_0 = -2.2259 \text{ MeV}$$

and

$$(H_{pn} - \varepsilon_k)\phi_l(k,\vec{r}) = 0\,, \quad \varepsilon_k = \frac{\hbar^2 k^2}{2\mu_r}\,, \tag{4}$$

where μ_r is the p-n reduced mass, ϕ_0 is the deuteron internal function and $\phi_l(k,\vec{r})$ the continuum state wave function of p-n pair with the linear and angular momenta $\hbar k$ and $l\hbar$, respectively.

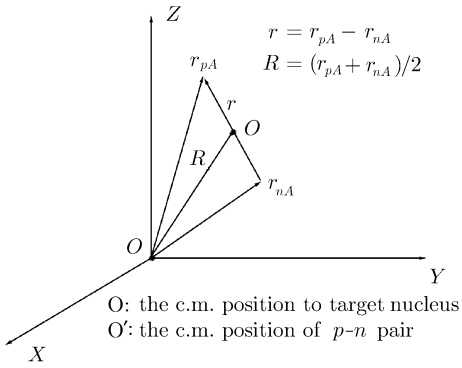

Fig. 1 The position vectors graph of the (n-p-A) system. $\boldsymbol{r}_{pA}$ is the coordinate of proton (p) relative to target nucleus A, $\boldsymbol{r}_{nA}$ is the coordinate of neutron (n) relative to A, $\boldsymbol{r}$ is the coordinate of p relative to n, and $\boldsymbol{R}$ is the coordinate of the center of mass of the p-n pair relative to A.

The three-body wave function $\psi_{JM}(\vec{R},\vec{r})$ can be expanded in terms of the p-n relative motion wave functions $\{\phi_0(\vec{r}), \phi_l(k,\vec{r})\}$ as

$$\psi_{JM}(\vec{R},\vec{r}) = \phi_0(r)\,\mathrm{Y}_{00}(\Omega_r)\,\mathrm{Y}_{JM}(\Omega_R)\chi_J(P_0,R)\frac{1}{R} + \int_0^\infty \sum_{l=0}^{\infty} \sum_{L=|J-l|}^{J+l} \big[\,\mathrm{Y}_l(\Omega_r) \otimes \mathrm{Y}_L(\Omega_R)\big]_{JM} \phi_l(k,r)\chi_{lLJ}(P_k,R)\frac{\mathrm{d}k}{R}\,, \tag{5}$$

where J is the total angular momentum quantum number of the $(A+2)$ system, M is the total angular momentum projection quantum number, and L is the orbital angular momentum quantum number of the p-n c.m. moving against target nucleus. The wave function $\chi_J(P_0,R)$ describes the p-n c.m. motion with the momentum $\hbar P_0$ in the elastic channel, and $\chi_{lLJ}(P_k,R)$ describes the p-n c.m. motion with the momentum $\hbar P_k$ in breakup channels. These momenta are determined by the conservation of the total energy, namely

$$E = \frac{\hbar^2 P_0^2}{2\mu_R} + \varepsilon_0 = \frac{\hbar^2 P_k^2}{2\mu_R} + \varepsilon_k\,, \tag{6}$$

where μ_R is the d-A reduced mass, and E is the total energy of the d-A system in their center of mass frame.

In CDCC, the model space needs to be truncated, the sum over l is truncated as $l \le l_{\max}$; the k integral as $k \le k_{\max}$, and setting the asymptotic outgoing wave boundary condition at $R = R_{\max}$. The average (AV) method[7] is used to discretizing k.

The $\hat{k}_i$ are defined as $\hat{k}_i^2 = (k_i + k_{i+1})^2/4 + \Delta^2/12$, and the momenta $\hbar\hat{k}_i$ and $\hbar\hat{P}_i$ satisfy the total energy conservation

$$E = \frac{\hbar^2 \hat{P}_i^2}{2\mu_R} + \frac{\hbar^2 \hat{k}_i^2}{2\mu_r}\,. \tag{7}$$

In this work, the channel number $\gamma = (i, J, l, L)$ increases according to the sequence (i, J, l, L), and in the following, $\hat{P}_\gamma \equiv \hat{P}_i$, $\hat{P}_0 \equiv P_0$. For all $\gamma = (i, J, l, L)$, including $\gamma_0 = (i = 0,\ J, l = 0,\ L = J)$, and γ_0 stands for the incoming channel. For some lower incoming deuteron energy, if $\hat{P}_i^2 < 0$ because of $\hbar^2\hat{k}_i^2/2\mu_r > E$, but $\hat{P}_{i-1}^2 > 0$, this channel $\gamma_d = (i, J, l, L)$ with $J = l = L = 0$ is called the first closed channel. All channels are open channels for $\gamma < \gamma_d$, and all channels are closed channels for $\gamma \ge \gamma_d$.

The wave function $\hat{\chi}_\gamma(\hat{P}_\gamma, R)$ is determined by a set of coupled channel equations:

$$\Big[\frac{\mathrm{d}^2}{\mathrm{d}R^2} + \hat{P}_\gamma^2 - \frac{L(L+1)}{R^2} + \frac{2\mu_R}{\hbar^2}V_{\gamma\gamma}(R)\Big]\hat{\chi}_\gamma(\hat{P}_\gamma, R) = \sum_{\gamma'\ne\gamma} \frac{2\mu_R}{\hbar^2}V_{\gamma\gamma'}(R)\hat{\chi}_{\gamma'}(\hat{P}_{\gamma'}, R)\,. \tag{8}$$

The matrix elements of coupling potentials $V_{\gamma\gamma'}(R)$ are obtained from $U_{nA}(\vec{r}_{nA})$ and $U_{pA}(\vec{r}_{pA})$.

When the incident energy is large enough and the closed channels does not appear, the coupled channel equations (8) are solved from $R = 0$ to $R_{\max}$ with step ΔR, the wave functions and their first derivatives in inner and outer region should be continuous at $R = R_{\max}$. However, if the closed channels is contained in coupled equations, the afore-mentioned calculation method is not suitable for solving equations (8) from $R = 0 \to R_{\max}$, because some exponential rising wave functions will be included. We can divide R into two space intervals: $R = 0 \to R_a \to R_{\max}$. R_a is about the nuclear radius and is taken as 12.0 fm in this work. The inner wave function is evaluated from $R = 0$ to R_a, and the nuclear potential is still present in $R = R_a \to R_{\max}$, and the outer wave function must be calculated from $R_{\max}$ to R_a . And

finally the inner and outer wave functions and their derivatives are joined at $R = R_a$, then the S-matrix elements are obtained for deriving the following physical quantities.

The differential elastic cross section is expressed as

$$\frac{\mathrm{d}\sigma}{\mathrm{d}\Omega} = \left| f_c(\theta) + \frac{1}{2\mathrm{i}\hat{P}_0} \sum_J (2J+1)\, \mathrm{e}^{2\mathrm{i}\sigma_J} (S^{(J)}_{\gamma_0,\gamma_0} - 1)\, \mathrm{P}_J(\cos(\theta)) \right|^2 . \tag{9}$$

The reaction cross section can be written as

$$\sigma_R = \frac{\pi}{\hat{P}_0^2} \sum_J (2\,J+1) \left(1 - |S^{(J)}_{\gamma_0,\gamma_0}|^2\right). \tag{10}$$

And the k-integrated partial breakup cross section is calculated with

$$\sigma^{(J)}_{b,l} = \frac{\pi(2J+1)}{\hat{P}_0^2} \sum_{L=|J-l|}^{J+l} \sum_{i=1}^{i_{\mathrm{open}}} \left| S^{(J)}_{\gamma,\gamma_0}(k_i) \right|^2 , \tag{11}$$

where i_{open} denotes the number of open channels. The partial-wave breakup cross section is defined by

$$\sigma_{b,l} = \sum_J \sigma^{(J)}_{b,l} . \tag{12}$$

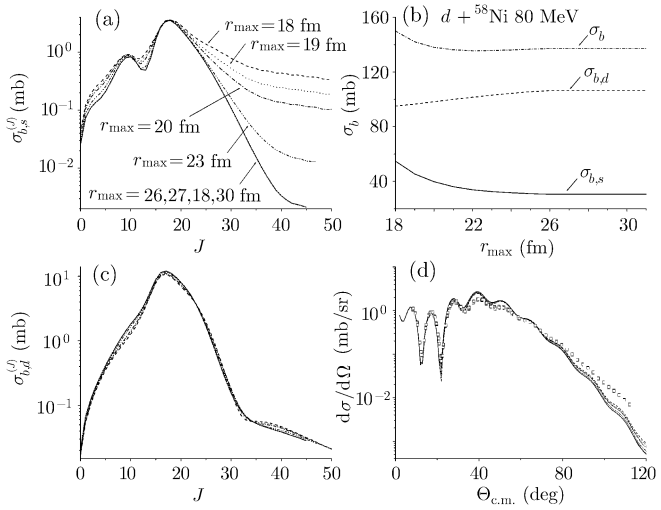

Fig. 2 Test of the validity of $r_{\max}$ truncation. For $d+{}^{58}$Ni at 80 MeV, with r ranging from 18 fm to 30 fm, the partial cross sections $\sigma^{(J)}_{b,s}$ and $\sigma^{(J)}_{b,d}$ with respect to J are plotted in (a) (b), respectively. The s-wave breakup cross section $\sigma_{b,s}$, the d-wave breakup cross section $\sigma_{b,d}$, and the total breakup cross section σ_b are plotted in (c). The elastic scattering angular distributions dσ/dΩ are plotted in (d) and the open dots in (d) are experimental data coming from Ref. [21]. In (a), (b), (d), the dashed lines represent r = 18 fm, dotted lines for r = 19 fm, dash-dotted lines for r = 20 fm, dash-dot-dotted lines for r = 23 fm, shot lines for r = 26 fm and the solid lines for r = 30 fm. All curves for $r \geq 26$ fm are overlapped each other.

Model Space Truncation As mentioned above, the model space truncation is generally composed of three types, namely, truncation of l, k, R. Some studies in Refs. [7] $\sim$ [9], [12], and [13] indicated that $k_{\max}$ = 1.0 fm^{-1}, $l_{\max}$ = 2 fm and $R_{\max}$ = 30 fm are sufficient truncations, and these three truncations are tested in this work. According to the work done with the test of the truncation of the p-n relative motion distance r, and $r_{\max}$ = 20 fm is widely used in CDCC calculations. But in this work we find that $r_{\max}$ = 20 fm is not enough, the maximum value of r should be increased to 27 fm, and this can be clearly seen from Fig. 2. For d + ^{58}Ni reaction at incoming energy 80 MeV, variations of $\sigma^{(J)}_{b,s}$ and $\sigma^{(J)}_{b,d}$ with J are plotted in Figs. (2a) and 2(b), the s-wave breakup cross section $\sigma_{b,s}$, the d-wave breakup cross section $\sigma_{b,d}$, and the total breakup cross section σ_b are plotted in Fig. 2(c), the elastic scattering angular distributions dσ/dΩ are plotted in Fig. 2(d). We can clearly see that with the increase of r, the $\sigma^{(J)}_{b,s}$ converges more quickly and remains steady at r = 26 fm, and the $\sigma_{b,s}$, $\sigma_{b,d}$, σ_b reach steady at around r = 26 fm. However, for $\sigma^{(J)}_{b,d}$ and dσ/dΩ, this tendency is not obvious. Thus, in practical CDCC calculations we choose $r_{\max}$ = 27 fm.

3 Calculate Results and Discussions

3.1 *Test of the Present Calculation Method*

Based on the CDCC approach and P3C5 algorithm,[22] we make a new code to consider the effect of deuteron breakup in nuclear reactions and the contribution of the closed channels. It is necessary to show the validity of our method. Besides testing the convergence of open channels, we also do with closed channels. We would like to make this convergence clear with two aspects. The first is the convergency of the k-integrated partial breakup cross section, and the second is the test of the convergency of the elastic scattering S-matrix element with respect to J. For $d+{}^{58}$Ni at 80 MeV and $d+{}^{16}$O at 10 MeV, figure 3 shows the convergence of $\sigma^{(J)}_{b,s}$, $\sigma^{(J)}_{b,d}$, imaginary part of the elastic S-matrix elements Im(S_J), and the real part Re(S_J). We can clearly find the perfect convergence for open channels (E_d = 80 MeV) and closed channels (E_d = 10 MeV) in Fig. 3, namely, both the $\sigma^{(J)}_{b,s}$ and $\sigma^{(J)}_{b,d}$ are convergent to zero in Fig. 3(a), the Im(S_J) to zero in Fig. 3(b) and the Re(S_J) to one in Fig. 3(c). These perfect convergencies mean that the present calculation method is valid.

3.2 *Contribution of Closed Channels*

In CDCC approach, when the p-n pair relative kinetic energy is greater than the total energy of the n-p-A three-body system, owing to the three-body system energy conservation, the closed channel with negative $\hat{P}_i^2$ is appeared. N. Austern pointed out that these closed channels couple strongly to the open channels, which contain outgoing flux; this kind of coupling affects the properties of open channels, and can make large contributions to the stripping cross section. The stripping is more sensitive than deuteron breakup to details of the three-body wave function; the stripping cross sections and the contribution of closed channels to it will be considered in the future. In this section, we would like firstly to observe the effects of the closed channels to the reaction cross sections σ_R,

breakup cross sections σ_b and elastic scattering angular distributions.

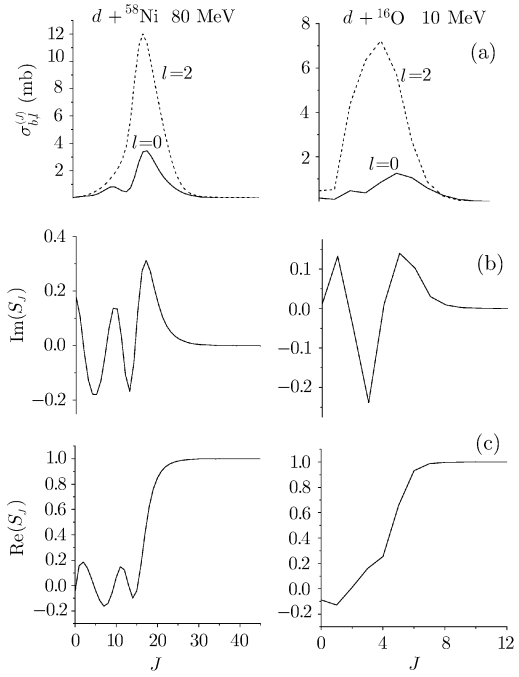

Fig. 3 Test of the convergence of our calculation method. The left side is for $d + {}^{58}$Ni at 80 MeV, and the right side is for $d + {}^{16}$O at 10 MeV, varying with the total angular momentum quantum number J, the k-integrated partial cross section $\sigma_{b,s}^{(J)}$ and $\sigma_{b,d}^{(J)}$ are plotted (a) with solid and dashed lines, respectively; The imaginary part of the elastic S-matrix elements are plotted in (b), and the real part in (c).

If we take $k_{\max} = 1.0$ fm^{-1} and $\Delta = 0.1$ fixed, the lower the incident energy is, the more closed channels appear. For example, according to the total energy conservation (7), if $E_d = 80$ MeV, we can get ten positive $\hat{P}_i^2$ ($i = 1 \sim 10$), this means that there are only ten open channels appearing and no closed channel appearing at 80 MeV; in the same way, nine open channels ($i = 1 \sim 9$) and one closed channel ($i = 10$) appears at 36 MeV, seven open channels ($i = 1 \sim 7$) and three closed channels ($i = 8 \sim 10$) appeared at 22 MeV, four open channels ($i = 1 \sim 4$) and six closed channels ($i = 5 \sim 10$) are appeared at 10 MeV, etc.

Figure 4 presents the contributions of the closed channels to reaction cross sections σ_R and breakup cross sections σ_b. For $d + {}^{58}$Ni at 10 MeV, with respect to the incident energy E_d increasing, the reaction cross sections and breakup cross sections without closed channels included in calculation $\sigma_R^{\text{non-closed}}$ and $\sigma_b^{\text{non-closed}}$ and those with closed channels included in calculation σ_R^{closed} and σ_b^{closed} are plotted, from which we can see that when the incident energy is larger than about 12 MeV, the $\sigma_R^{\text{non-closed}}$ and σ_R^{closed} can hardly be distinguished from each other, and so $\sigma_b^{\text{non-closed}}$ and σ_b^{closed} are. For the energy range lower than about 12 MeV, the $\sigma_R^{\text{non-closed}}$ and $\sigma_b^{\text{non-closed}}$ are larger than σ_R^{closed} and σ_b^{closed}, respectively. These mean that the contribution of closed channels to σ_R and σ_b can be ignored when incident energy is larger than about 12 MeV, and the closed channels reduce the σ_R and σ_b when incoming energy is lower than about 12 MeV. It should be noted that both the $\sigma_b^{\text{non-closed}}$ and σ_b^{closed} have a peak value around 12 MeV, and this means that the peak value does not depend on exclusion or inclusion of the contribution of the closed channels. However, such a peak value structure does not appear in σ_R in this case ($d + {}^{58}$Ni).

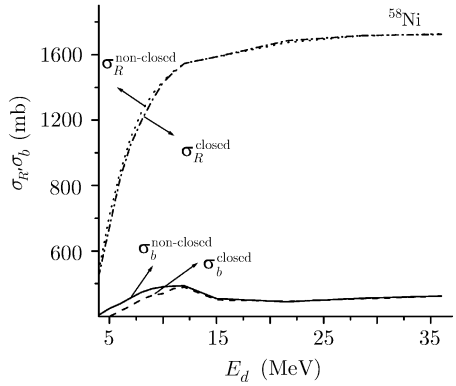

Fig. 4 The contribution of closed channels to the reaction cross sections and breakup cross sections. For $d + {}^{58}$Ni, with respect to the incident energy E_d increasing, the breakup cross sections without closed channels $\sigma_b^{\text{non-closed}}$ and with closed channels σ_b^{closed} are plotted with solid and dashed lines, respectively; and the reaction cross sections without closed channels $\sigma_R^{\text{non-closed}}$ and with closed channels σ_R^{closed} are plotted with dotted and dash-dotted lines.

With incident deuteron energy varying from 4 MeV to 36 MeV, the elastic scattering angular distributions of ^{58}Ni from this work with and without the contribution of closed channels are plotted in Fig. 5. For $E_d = 4$ MeV and $E_d = 36$ MeV, seven and one closed channels occur, respectively. From Fig. 5 we can see that, for lower incident deuteron energy ($4 \sim 7$ MeV), the elastic scattering angular distributions with the contribution of closed channels are with less fluctuations than those without the contribution of closed channels, and the former seems more rational than the later in physics. We can also clearly find that, with the E_d increase and larger than 12 MeV, the angular distributions of the cases with and without closed channels are close to each other, and can hardly be distinguished about 30 MeV. Generally speaking, for incident energies larger than about 12 MeV, it is a good idea to calculate the σ_R, σ_b and elastic scattering angular distributions by neglecting the very small effects of the closed channels. This will reduce the computational burden.

3.3 *Comparison of Elastic Scattering Angular Distribution*

Because the global potential parameters[1] can reproduce the experimental data well in a wide (Z, A) and energy range, it is feasible to compare the results of the CDCC with those from the global potential parameters. In this way, the effects of the deuteron breakup process on elastic scattering angular distributions and reaction cross

sections are more systematically studied for many target nuclei in a wide region of energies.

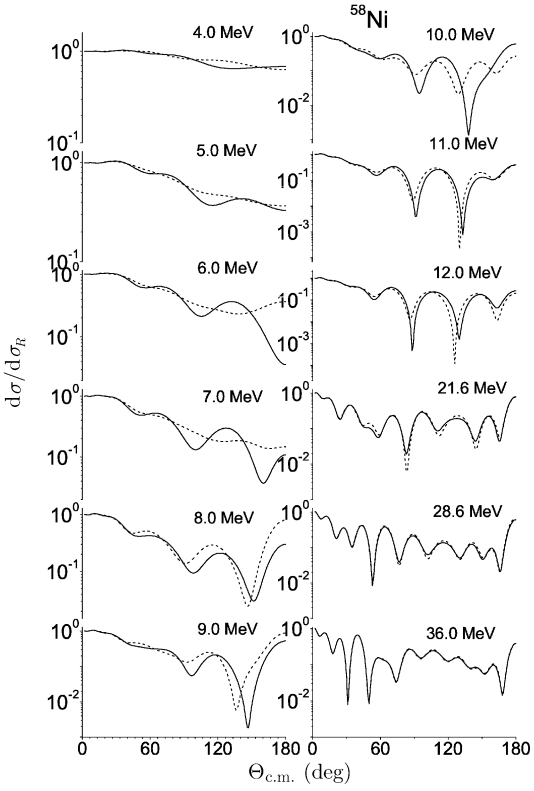

Fig. 5 Comparison of the elastic scattering angular distributions of this work without and with the contribution of closed channels. The solid line and dashed line describe this work without and with closed channels, respectively.

According to the above analyses, the effects of the closed channels are not considered in this part in the energy range larger than about 12 MeV. The calculated elastic scattering angular distributions from global potential, this work and Ref. [6] are plotted in Fig. 6.

There are mainly three differences between this work and Ref. [6] firstly, the Coulomb potential in Eq. (1), we perform calculations by evaluating Coulomb interaction at r_p and that of Ref. [6] at R; secondly, for the $V_{pn}(\vec{r})$, in Ref. [6], the values of r_0 and v_0 are taken as 1.484 fm and 72.15 MeV, respectively; In order to make the calculating deuteron binding energy in better accordance with its experimental value, we change v_0 to 72.194 MeV; thirdly, for solving the coupled channel equations (8), the P3C5 algorithm is used in this work, the error of this algorithm is of $O(h^6)$, and that of the B-splines method adopted in Ref. [6] is $O(h^3)$, this means that the present work has a higher calculation precision than that of Ref. [6].

From Fig. 6 we can find that, generally speaking, the CDCC results cannot reproduce the experimental data well as those from our global potentials, and our CDCC results are a little better than those of Ref. [6]. Some fluctuations appear in CDCC results relative to those of the global potentials, and we believe this phenomenon comes from the effects of break-up channels on elastic channel and no spin-orbit potentials in consideration. Besides, there are no free parameters included in the CDCC calculations, therefore, the results of CDCC are physically acceptable and reasonable in comparison with the experimental data.

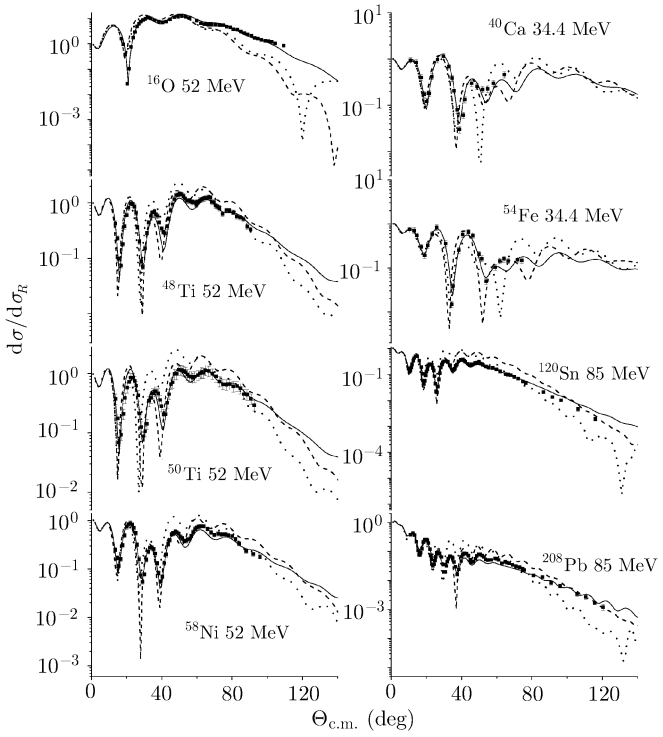

Fig. 6 Comparison of elastic scattering angular distributions among global potential, this work and P. Chau Huu-Tai[6] results. The results using global potential, this work and Ref. [6] are plotted as solid, dashed and dotted lines. The experimental data are from Refs. [5], [23], and [24].

3.4 *Reaction Cross Section and Breakup Cross Section*

The reaction cross sections σ_R and breakup cross sections σ_b of ^{16}O, ^{40}Ca, ^{58}Ni, ^{90}Zr, ^{120}Sn, and ^{208}Pb are drawn in Fig. 7. From this figure we can find that, besides ^{208}Pb, the σ_R of this work is in better agreement with the experimental data than those of P. Chau Huu-Tai[6] for low incident energy, and with the increase of the energy the two curves are very close to each other. This figure reveals that the deuteron breakup process causes effect in reaction cross sections. It increases σ_R in the energy region below 80 MeV for the light nuclei and below 100 MeV for medium nuclei, then it decreases σ_R for higher energies. However it decreases σ_R for heavy nuclei in nearly the whole energy range.

In Subsec. 3.2, we have already pointed out that for ^{58}Ni, there is a peak structure in σ_b around 12 MeV, but such a peak structure does not appear in σ_R (Fig. 4). From Fig. 7 we can clearly see that similar phenomena exist for all the target nuclei ranging from ^{16}O to ^{208}Pb, and the peak in σ_b is the highest for ^{40}Ca and ^{58}Ni, while it gradually decrease as the target becomes lighter or heavier. This means that the peak structure in σ_b around 12 MeV not only exists for a special nucleus but also appears in a wide range of nuclei. This structure indeed exists, but at this moment we do not yet understand what the reason is

for this peak structure in σ_b.

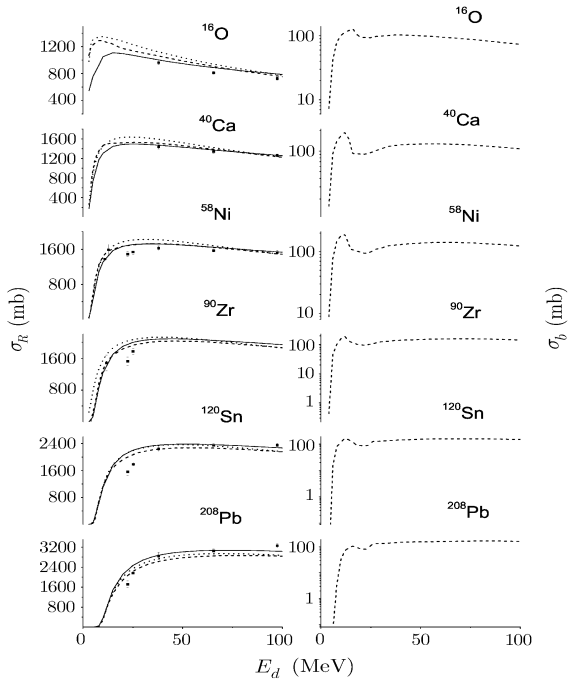

Fig. 7 The reaction cross sections varying with incident energy E_d are plotted in the left side, and the results from global potential, this work and Ref. [6] are plotted as solid, dashed and dotted lines, respectively, the experimental data of reaction cross sections are from Refs. [25] $\sim$ [28]. Varying with E_d, the breakup cross sections are plotted in the right side with dashed line.

4 Summary

Based on the CDCC approach and the P3C5 algorithm, a new code is developed to observe the effects of deuteron breakup on the reaction cross sections and elastic scattering angular distributions below 200 MeV, with target nuclei ranging from ^{12}C to ^{208}Pb. The contributions of the closed channels to breakup cross sections, reaction cross sections and elastic scattering angular distributions are also considered. The convergence of the calculations with our new code are checked for both situations of only with open channels and also included closed channels.

The effects of deuteron breakup on the reaction cross sections vary with the incident energy and target mass. Comparing the experimental data and the results from our global potential, the elastic scattering angular distributions in CDCC show some fluctuation for low incident energies, and this phenomenon gradually disappears with the energy increasing and a good agreement with experimental data is achieved. For the target nuclei ranging from ^{12}C to ^{208}Pb, there is a peak value structure in breakup cross sections around 12 MeV.

The calculations including closed channels reduce the reaction cross sections σ_R and breakup cross sections σ_b when incoming energy is lower than about 12 MeV, and its effects on σ_R and σ_b are indistinctive and can be neglected when incident energy is larger than about 12 MeV. With incident energy increasing, the effects of closed channels gradually become weakly on the elastic scattering angular distributions, and the effects nearly disappear about 30 MeV.

With the incident deuteron energy increasing, the effects of closed channels on σ_R, σ_b, and the elastic scattering angular distributions decrease, and these phenomena are physically reasonable. As the incident deuteron energy increases, the relative kinetic energy between p and n gradually decreases its importance in comparison with the total energy of the three-body system, so the effects of deuteron breakup channels gradually become weaker in comparison with the dynamics of the deuteron as a whole moving against the target.

References

[1] H.X. An and C.H. Cai, Phys. Rev. C **73** (2006) 054605.
[2] Y.L. Han, Y.Y. Shi, and Q.B. Shen, Phys. Rev. C **74** (2006) 044615.
[3] C.M. Perey and F.G. Perey, At. Data Nucl. Data Tables **13** (1974) 293; **17** (1974) 1.
[4] W.W. Daehnick, J.D. Childs, and A. Vrcelj, Phys. Rev. C **21** (1980) 2253.
[5] J. Bojowald, *et al.*, Phys. Rev. C **38** (1988) 1153.
[6] P. Chau Huu-Tai, Nucl. Phys. A **773** (2006) 56.
[7] N. Austern, *et al.*, Phys. Rep. **154** (1987) 125.
[8] R.A.D. Piyadasa, M. Kawai, M. Kamimura, and M. Yahiro, Phys. Rev. C **60** (1999) 044611.
[9] M. Yahiro, M. Nakano, Y. Iseri, and M. Kamimura, Prog. Theor. Phys. **67** (1982) 1467.
[10] M. Kamimura, *et al.*, Prog. Theor. Phys. Suppl. **89** (1986) 1.
[11] M. Yahiro and M. Kamimura, Prog. Theor. Phys. **65** (1981) 2046.
[12] R.A.D. Piyadasa, *et al.*, Prog. Theor. Phys. **81** (1989) 910.
[13] M. Yahiro and M. Kamimura, Prog. Theor. Phys. **65** (1981) 2051.
[14] H. Amakawa and K. Yazaki, Phys. Lett. B **87** (1979) 159.
[15] H. Amakawa and T. Tamura, Phys. Rev. C **26** (1982) 904.
[16] H. Amakawa, A. Mori, H. Nishioka, K. Yazaki, and S. Yamaji, Phys. Rev. C **23** (1981) 583.
[17] T. Egami, *et al.*, Phys. Rev. C **70** (2004) 047604.
[18] F.M. Nunes, *et al.*, Nucl. Phys. A **736** (2004) 255.
[19] M. Yahiro, H. Kameyama, Y. Iseri, M. Kamimura, and M. Kawai, Nucl. Lett. B **182** (1986) 135.
[20] A.J. Koning and J.P. Delaroche, Nucl. Phys. A **713** (2003) 3–4, 231–310.
[21] E.J. Stephenson, *et al.*, Phys. Rev. C **10** (1974) 217.
[22] N.M. Clarke, J. Phys. G: Nucl. Phys. **10** (1984) 1535.
[23] E. Newman, L.C. Becker, and B.M. Freedom, Nucl. Phys. A **100** (1967) 225.
[24] F. Hinterberger, G. Mairle, U. Schmidt-Rohr, G.J. Wagner, and P. Turek, Nucl. Phys. A **111** (1968) 265.
[25] A. Auce, *et al.*, Phys. Rev. C **53** (1996) 2919.
[26] S. Mayo, W. Schimmerling, M.J. Sametband, and R.M. Eisberg, Nucl. Phys. **62** (1965) 393.
[27] A. Budzanowski and K. Growski, Phys. Lett. **2** (1962) 280.
[28] K. Bearpark, W.R. Graham, and G. Jones, Nucl. Phys. **73** (1965) 206.